J Neurophysiol 95: 2617–2629, 2006.
First published January 25, 2006; doi:10.1152/jn.01287.2005.

Representation of Auditory Signals in the M-Cell: Role of Electrical Synapses

T. M. Szabo, S. A. Weiss, D. S. Faber,* and T. Preuss*
Department of Neuroscience, Albert Einstein College of Medicine, Bronx, New York

Submitted 7 December 2005; accepted in final form 18 January 2006

Szabo, T. M., S. A. Weiss, D. S. Faber, and T. Preuss. Representation of auditory signals in the M-cell: role of electrical synapses. *J Neurophysiol* 95: 2617–2629, 2006. First published January 25, 2006; doi:10.1152/jn.01287.2005. The teleost Mauthner (M-) cell mediates a sound-evoked escape behavior. A major component of the auditory input is transmitted by large myelinated club endings of the posterior VIIIth nerve. Paradoxically, although nerve stimulations revealed these afferents have mixed electrical and glutamatergic synapses on the M-cell's distal lateral dendrite, paired pre- and postsynaptic recordings indicated most individual connections are chemically silent. To determine the sensory information encoded and the relative contributions of these two transmission modes, M-cell responses to acoustic stimuli in air were recorded intracellularly. Excitatory postsynaptic potentials (EPSPs) evoked by both short 100- to 900-Hz "pips" and longer-lasting amplitude- and frequency-modulated sounds were dominated by fast, repetitive EPSPs superimposed on an underlying slow depolarization. Fast EPSPs *1*) have kinetics comparable to presynaptic action potentials, *2*) are maximal on the distal lateral dendrite, and *3*) are insensitive to GluR antagonists. They presumably are coupling potentials, and power spectral analysis indicated they constitute a high-pass signal that accurately tracks sound frequency and amplitude. The spatial profile of the slow EPSP suggests both proximal and distal dendritic sources, a result supported by predictions of a multicompartmental model and the effects of AMPAR antagonists, which preferentially reduced the proximal component. Thus a second class of afferents generates a portion of the slow EPSP that, with sound stimuli, demonstrate that the dominant mode of transmission at LMCE synapses is electrical. The slow EPSP is a dynamic, low-pass representation of stimulus strength. Accordingly, amplitude and phase information, which are segregated in other systems, are faithfully represented in the M-cell.

INTRODUCTION

Electrical synapses are commonly assumed to mediate rapid transmission and synchronization of neuronal populations (Bennett and Zukin 2004; Connors and Long 2004; Thomson 2000). In fact, studies in many systems, particularly invertebrates, have shown that these synapses might have more specific functions, such as modifying neuronal oscillations (Kepler et al. 1990) and coincidence detection (Edwards et al. 1998). Less clear, however, are the respective roles of electrical and chemical synapses in complex information processing in cases where these two modes of synaptic transmission coexist (i.e., at mixed synapses). The best examples thus far are in invertebrates, where these two components often have opposing excitatory and inhibitory actions (Johnson et al. 1993; Sharp et al. 1992).

In goldfish, the monosynaptic excitatory connection between posterior eighth nerve afferents, called large myelinated club endings (LMCEs), and an identified second-order reticulospinal neuron, the Mauthner (M-) cell, is mediated by mixed electrical and chemical synapses (see Pereda et al. 2004; Zottoli and Faber 2000). The afferents are excited by hair cells in the sacculus that are responsive to acoustic pressure (Furukawa and Ishii 1967). They transmit this auditory information to the M-cell, which in turn triggers the startle response (Zottoli 1977). Because a great deal of information about the basic properties of these synapses has been generated and these afferents are selectively activated by sounds in air, it is an ideal system for defining the different functional roles of their electrical and chemical components during sound reception. However, evidence from paired recordings suggests that >80% of the connections are chemically silent (Lin and Faber 1988a); that is, a presynaptic action potential produces a postsynaptic coupling potential, the sign of electrical transmission, but no chemically mediated excitatory postsynaptic potential (EPSP). It has been shown that glutamatergic transmission is unmasked by modulations of the presynaptic action potential waveform (Lin and Faber 1988b) and might be recruited when a large fraction of the afferent population is coactivated (Pereda et al. 2004). Thus these properties also raise the question of whether, and under what conditions, the chemical synapses contribute to the processing of auditory information.

We report here results of studies that used acoustic stimuli in air comparable in intensity to those that can elicit an M-cell–mediated escape in free-swimming fish under water, specifically abrupt, loud sound pips and longer lasting amplitude- (AM) and frequency-modulated (FM) tone bursts. Applying the stimuli in air involves only the pressure component of sound (Fay and Popper 1999) and therefore selectively activates the input to the M-cell from the posterior VIIIth nerve, including the club endings. Our results demonstrate that the M-cell responses to these stimuli have two components: fast, repetitive EPSPs superimposed on a depolarizing envelope, which we call a slow EPSP. The spatial distribution of the fast EPSPs along the dendrite combined with pharmacological data and results from a multicompartment simulation of the M-cell indicate that they are electrical coupling potentials resulting from impulses in the club endings. In contrast, the slow EPSP is not composed of discrete chemical EPSPs and is generated by synapses on both the soma and proximal dendrite. There is no evidence for a significant glutamatergic component generated at the club ending synapses under the stimulus conditions we used. Power spectral analysis of the responses to the modulated stimuli suggests the electrical synapses encode both stimulus frequency and amplitude in the fast EPSP, whereas

* D. S. Faber and T. Preuss contributed equally to this work.

Address for reprint requests and other correspondence: T. Preuss, Department of Neuroscience, Albert Einstein College of Medicine, 1300 Morris Park Ave., Bronx, NY 10461 (E-mail: tpreuss@aecom.yu.edu).

The costs of publication of this article were defrayed in part by the payment of page charges. The article must therefore be hereby marked "*advertisement*" in accordance with 18 U.S.C. Section 1734 solely to indicate this fact.

the slow EPSP is a smoothly graded function of the envelope of sound amplitude.

METHODS

Animals and preparations

Goldfish (*Carassius auratis*, length 4–6 in.) were obtained from EECHO Systems (North Kansas City, MO), Hunting Creek Fisheries (Thurmond, MD), and Billy Bland Fisheries (Taylor, AR). They were maintained on a controlled photoperiod of 12 h light/dark at 18°C in recirculating, aerated water (Preuss and Faber 2003). Water was conditioned with NovAqua (0.13 ml/l; Novalek, Hayward, CA), Coppersafe (0.4 ml/l; St. John Laboratories, Harbor City, CA), Instant Ocean (70 mg/l; Aquarium Systems, Mentor, OH), Aquarium Salt (190 mg/l; Jungle Laboratories, Cibolo, TX), and Proper pH (350 mg/l; Aquarium Pharmaceuticals, Chalfont, PA). Fish were initially anesthetized with 100 mg/l 3-aminobenzoic acid ethyl ester (MS-222; Sigma, St. Louis, MO), then further anesthetized in ice water. Fish were then mounted in a recording chamber and respirated with aerated water flowing through the mouth and out over the gills. The water contained 60 mg/l MS-222 and was maintained at 18°C using a Delta Star Chiller (Aqua Logic, San Diego, CA). After exposure of the spinal cord for M-cell antidromic stimulation, and of the midbrain for intracellular recordings (Faber and Korn 1978), the fish was immobilized with *d*-tubocurarine (1 μg/g body weight; Sigma) injected intramuscularly and the brain was superfused with normal fish saline (in mM: 124.0 NaCl, 5.1 KCl, 2.8 $NaH_2PO_4 \cdot H_2O$, 0.9 $MgSO_4$, 1.6 $CaCl_2 \cdot 2H_2O$, 5.6 glucose, and 20.0 HEPES, pH 7.2). In experiments designed to block specific glutamatergic receptors, saline contained one or more of the following.

1) *N*-Methyl-D-aspartate (NMDA) receptor antagonists:100–200 μM D-(−)- and DL-2-amino-5-phosphonovaleric acid (APV; Sigma, St. Louis, MO; Tocris, Ellisville, MO), 100–150 μM 3-((*R*)-2-carboxypiperazin-4-yl)-propyl-1-phosphonic acid (CPP; Tocris).

2) α-Amino-3-hydroxy-5-methyl-4-isoxazolepropionic acid (AMPA)/kainate receptor antagonists: 100–150 μM 6-cyano-7-nitroquinoxaline-2,3-dione disodium (CNQX; Sigma, Tocris) and 100 μM 2,3-dioxo-6-nitro-1,2,3,4-tetrahydrobenzo[f]quinoxaline-7-sulfonamide disodium salt (NBQX; Tocris).

3) Metabotropic glutamate receptor (mGluR) antagonists: Group I/II (nonselective): 1 mM (*S*)-α-methyl-4-carboxyphenylglycine (MCPG; Tocris), Group II (selective): 1 mM (2*S*)-2-amino-2-[(1*S*,2*S*)-2-carboxycycloprop-1-yl]-3-(xanth-9-yl) propanoic acid (LY 341495; Tocris), Group III (selective): 200 μM (*RS*)-α-methylserine-*O*-phosphate (MSOP, Tocris).

Electrophysiological recordings

Recording procedures and identification of the M-cell were previously described (Faber and Korn 1978). M-cell intracellular responses to sound as well as to posterior eighth nerve (orthodromic) and spinal cord (antidromic) stimulation were recorded from the soma (50 μm lateral to the axon cap) and distally along the cell's lateral dendrite $\leq$400 μm from the axon cap, using 4- to 7-MΩ microelectrodes filled with 5 M potassium acetate (KAc). The axon cap is the region surrounding the axon-hillock and initial segment of the axon. All recordings were performed in current clamp (Axoclamp-2B, Axon Instruments, Foster City, CA). In all experiments reported here, resting membrane potential was in the range of −76 to −83 mV in both the soma and dendrite and did not vary by more than 5 mV during a recording session. Similarly, the size of the M-cell's antidromic action potential varied by no more than 5% during control recordings. Because the IPSP equilibrium potential equals the resting membrane potential of the M-cell (Furukawa and Furshpan 1963), inhibitory postsynaptic potentials (IPSPs) were not manifest as frank membrane potential changes unless the cell was significantly depolarized.

Extracellular recording techniques

In a series of experiments, the posterior eighth nerve was exposed surgically and extracellular recordings of evoked multiunit activity were obtained with a 100-μm stainless steel electrode open at its tip (impedance $\approx$ 40 kΩ) connected to a high-gain AC amplifier (A-M Systems, Carlsborg, WA). These data were collected for comparison with simultaneously collected intracellular responses as a control that the pharmacological agents had minimal effect at the level of the hair cell synapses.

Acoustic stimuli

All stimuli were applied in air (dB re:20 μPa) through three speakers: two tweeters located about 40 cm symmetrically in front and to the left and right of the fish's head, and a subwoofer located about 35 cm above and in front of the fish (CA-3550 "Platinum Series" speakers, Cyber Acoustics, LLC, Vancouver, WA). Because the fish and the speakers were out of the water, only the pressure component of the stimulus was detected by the fish and transmitted to the inner ear from the swim bladder by the Webberian ossicles (Popper and Platt 1993). Custom-designed software for a Macintosh G4 in combination with an AD card (National Instruments, Austin, TX) was used to generate digital sound stimuli, as well as to collect and analyze data.

Two types of acoustic stimuli were used.

1) Short "pip" stimuli, or one cycle of a sine wave, ranging from 100 to 900 Hz.

2) Longer-lasting (100 to 200 ms) AM and AM/FM stimuli, defined as amplitude-modulated sounds that increased linearly in intensity with time, and were either constant frequency (AM) or also frequency-modulated (AM/FM), respectively. The FM followed an exponential algorithm.

[Note: The loudspeakers did not precisely follow the short duration of the pip sound stimulus; i.e., pips lasted longer than the duration of one sine wave as a result of speaker membrane inertia and reverberations. However, measurements of the sound demonstrated that the initial sine-wave frequency faithfully represented the command frequency. The modulated signals more accurately represented the stimulus waveform because they increased in amplitude gradually.] The final intensity of the sound stimuli ranged from 66 to 114 dB, as measured with a sound level meter (72–860, Tenma, Springboro, OH). Sound signals were recorded approximately 6 cm above the fish's head using a microphone (Radio Shack, Ft. Worth, TX).

Modeling studies

The Neuron simulation package (Yale, New Haven, CT) was used to implement a multicompartment model of the M-cell. The modeled cell possessed 15 segmented compartments, based on earlier morphological studies of the goldfish M-cell (Bodian 1952; Zottoli 1978) and an equivalent circuit model of the cell constructed by Furukawa (1966). The widths of the compartments were tapered to provide realistic continuity between compartments. Because this model was used to compare experimental data with predictions based on the passive membrane properties of the M-cell soma and primary dendrites, the axon was not included in the simulation. Internal resistivity was assumed to be 100 Ω/cm. Previous estimates of the cell's specific membrane capacitance were in the range of 2.5 μF/cm^2 with an input resistance of about 100 kΩ (Furukawa 1966). However, more recent measurements suggest values of the latter are $\geq$200 kΩ, with a membrane time constant of $<$0.5 ms (Preuss and Faber 2003). Therefore we set specific membrane capacitance at 1 μF/cm^2, a value consistent with measurements for most biological membranes (Segev

and Burke 1998). The uniform passive specific membrane resistance was calculated by iteratively measuring the input resistance and time constant of the M-cell for specific membrane resistance values ranging from 100 to 1,000 Ω/cm^2 (Segev and Burke 1998) and by matching the waveform of the antidromic action potential and its experimentally observed passive soma–dendritic decremental conduction. The best fit was obtained with an input resistance of about 250 kΩ and a time constant of about 200 μs in the soma. Synaptic currents were modeled by injecting a dynamic voltage clamp at a single point on the dendrite of the model M-cell, using the experimentally recorded responses as the clamp input. Model responses were calculated using a backward Euler numerical integration method.

Data analysis

All measurements of signal amplitudes and kinetics were made on averaged responses ($n \geq 8$) using either in-house software, IGOR Pro (Wavemetrics, Lake Oswego, OR) or LabView 7.0 (National Instruments, Austin, TX). To analyze high- and low-frequency signal components separately, averaged recordings were passed through a sixth-order digital Butterworth filter, with a high-frequency cutoff at 60 Hz, or a second-order digital Butterworth filter with a low-frequency cutoff at 60 Hz, respectively. Power spectral densities were calculated with a Fourier transform algorithm, and the signal energy in a joint time–frequency spectrogram (JTFS) was calculated using a short-time Fourier transform with a 40-ms rectangular window shifted in 1-ms increments. To quantify power versus time plots, power was calculated from the JTFS by summating the total power in the 0- to 2,000-Hz band in time increments of 1 ms. The last 25 ms of the sounds and the M-cell responses were poorly represented by the JTFS because of the sliding window algorithm and were not used. The high-pass–filtered response and the unfiltered extracellular recordings from the posterior VIIIth nerve were normalized for DC offset before calculation of root-mean-squared (RMS) values. To further compare the filtered signals with the acoustic stimuli, the amplitude envelopes of the sounds and the high-pass–filtered M-cell responses (HP PSPs) were approximated by finding the successive maxima for each within optimal intervals from 0 to 175 ms. The time course and amplitude of these maxima were fit with sixth-order polynomials. When the power of the sound was plotted instead, it was fit by a sixth-order polynomial at all points. Comparisons between the different response representations and stimulus intensity or power were made after scaling the corresponding fits with an optimal multiplier derived by minimization of the mean square error between the two curves. Linear regression analysis of these relationships was performed by comparing the scaled values of the points only at the time points used for deriving the polynomial fits. All traces shown here represent an average of eight to ten individual responses and values of n refer to the number of fish unless otherwise noted. All statistics represent two-tailed, paired Student's t-test unless otherwise noted. Results are presented as mean $\pm$ SE.

RESULTS

Characterization of the M-cell response to short sound "pips"

Because sound stimuli were applied in air we were able to isolate their pressure component. Sound pressure is transmitted from the swim bladder to the sacculus, whose hair cells synapse with fibers of the posterior branch of the eighth nerve (VIIIp). The VIIIp fibers, in turn, terminate on the distal lateral dendrite of the M-cell approximately 250–400 μm from the axon cap as large myelinated club endings where they form mixed electrical and chemical synaptic contacts (Bodian 1952; Lin and Faber 1988a; Lin et al. 1983; Tuttle et al. 1986). Estimates based on both morphological and electrophysiological data suggest that about 75 to 100 club endings (average diameter about 10 μm) terminate on the dendrite (about 20 μm in diameter) in this region. As shown in Fig. 1 for a 200-Hz sound "pip," simultaneous extracellular recordings from posterior VIIIth nerve afferents and intracellular recordings from the M-cell suggest that presynaptic spike activity is correlated with high-frequency, relatively synchronous, spikelike transients in the postsynaptic cell, which we call the fast EPSP. These latter events are superimposed on an underlying, depolarizing envelope, the slow EPSP. The experiments described below were designed to identify the origin of sound-evoked EPSPs, focusing first on responses to sound pips.

Because initial experiments indicated that pip-evoked responses were maximal in amplitude at distal locations on the dendrite, frequency and amplitude dependencies of the fast and slow EPSPs were characterized 350 μm distal to the M-cell's axon cap. Successive fast EPSP peaks were designated P1, P2, and so forth (Fig. 2). They were found to have kinetics similar to those of action potentials; i.e., the rise time and half-width of P1 were 0.24 $\pm$ 0.02 ms ($n = 5$) and 0.43 $\pm$ 0.04 ms ($n = 10$), respectively. It was previously shown that coupling potentials evoked in the M-cell by the firing of a single club ending have a half-width of approximately 0.275 ms, whereas the half-width of the later chemical EPSP is about 1.5–2.0 ms (Lin and Faber 1988b). Thus the fast EPSPs seen in these sound-evoked responses were most likely mediated by current flow across the

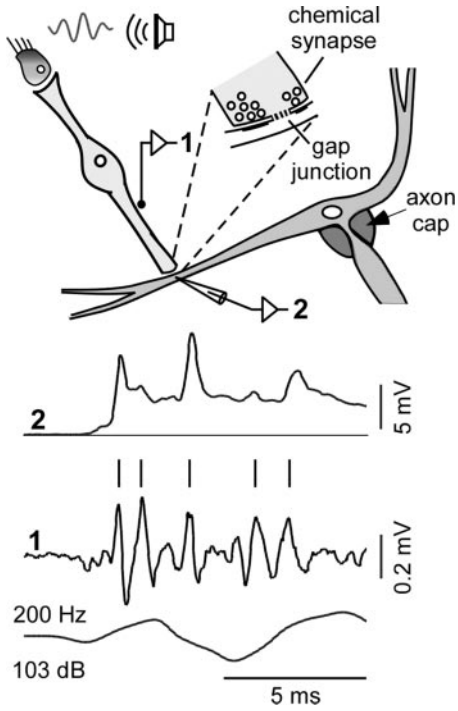

FIG. 1. Characteristics of sound-evoked responses in the Mauthner (M-) cell and its afferents. *Top*: schematic of an VIIIp afferent and the M-cell, with the indicated recording sites on the nerve (1) and the lateral dendrite (2). *Inset*: individual club endings of VIIIp afferents have electrical and chemical synapses with the lateral dendrite. *Bottom*: simultaneous recordings of compound action potentials in VIIIp afferents (1, extracellular) and the M-cell lateral dendrite (2, intracellular) evoked by a sound "pip" (*bottom trace*: microphone recording). Note: repetitive activity in the VIIIth nerve (1) during the sound stimulus is correlated (vertical lines) with a complex excitatory postsynaptic potential (EPSP) in the M-cell (2).

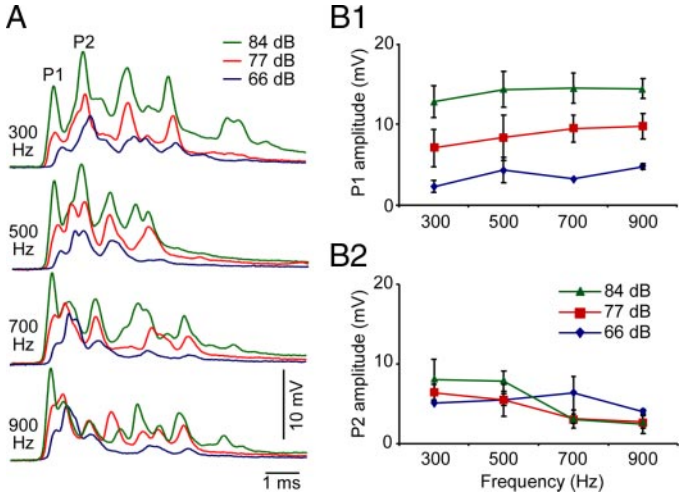

FIG. 2. Differential effects of sound frequency and intensity on EPSPs evoked in the M-cell. *A*: sample EPSPs recorded 350 μm lateral to the axon cap and evoked by sound pips of the indicated frequencies. In each panel, responses to 66, 77, and 84 dB are superimposed. P1 and P2 designate the first 2 EPSP peaks. *B1* and *B2*: plots of P1 and P2 amplitude (ordinates), respectively, vs. stimulus frequency (abscissas) for 66, 77, and 84 dB (66 dB, $n = 2$; 77 and 84 dB, $n = 5$). P1 amplitude is intensity dependent and frequency independent, whereas P2 is most sensitive to low frequencies.

electrical synapses. The presence of clear peaks in these responses implies a high degree of synchrony in the afferents, as also seen with extracellular nerve recordings (Fig. 1).

To further characterize M-cell responses to short sounds, both stimulus intensity and frequency were varied while dendritic responses to pips were recorded (Fig. 2*A*). The amplitude of P1 varied with intensity for a given frequency, but appeared to be frequency independent for a given decibel level in the range tested (Fig. 2*B1*). This apparent intensity sensitivity of P1 is consistent with synchronized recruitment of more afferents. In addition, the onset latency of P1, which was in the range of 1–2 ms, decreased with increasing sound intensity (e.g., Fig. 2*A*). P1 onset was, on average, 0.25 ± 0.03 ms earlier at 84 than at 77 dB ($n = 5$). A similar intensity dependency of EPSP latency was previously described (e.g., Casagrand et al. 1999). This onset latency is within the 2- to 3-ms temporal window during which the M-cell either does or does not trigger an escape (Preuss and Faber 2003). In contrast to P1, the amplitude of P2, measured from trough to peak, appeared to be maximal at low frequencies, but did not appear to be intensity dependent (Fig. 2*B2*). This apparent lack of intensity dependency might be the consequence of an overlapping feedforward inhibition (Oda et al. 1998; Preuss and Faber 2003) that would shunt P2. Finally, for a given intensity, the interval between P1 and P2 decreased as a function of frequency ($n = 5$), suggesting a tendency of the fast EPSPs to follow stimulus frequency or its harmonics. This property is analyzed in more detail for responses to long-lasting amplitude- and frequency-modulated sounds (see following text).

The pip-evoked EPSP originates on the distal lateral dendrite

Because it is possible to record sequentially from the M-cell soma and identified dendritic loci, the passive spread of the antidromically generated action potential and that of the mixed electrical and chemical EPSP evoked by stimulation of VIIIp have been studied extensively (see Faber and Korn 1978; Preuss and Faber 2003). Both have spatial profiles consistent with their sites of origin and dendritic cable properties (Fig. 3*A*). If pip-evoked EPSPs in the M-cell arise from activation of the large myelinated club endings, responses should be maximal in amplitude at the postsynaptic region where these afferents terminate, i.e., 250–400 μm distal from the axon cap. Correspondingly, the amplitude of these responses should become smaller at recording sites farther from the club endings and closer to the soma, according to the cable properties of the M-cell dendrite. This prediction was confirmed in four experiments with recordings of the fast sound-evoked peaks at four sites along the lateral dendrite and the soma (e.g., Fig. 3*B1*). In addition, this spatial distribution was not frequency dependent, as shown in the example of Fig. 3*B2*. The fact that, in some cases, P1 amplitude was essentially the same for the two distalmost recording sites suggested a distributed input span-

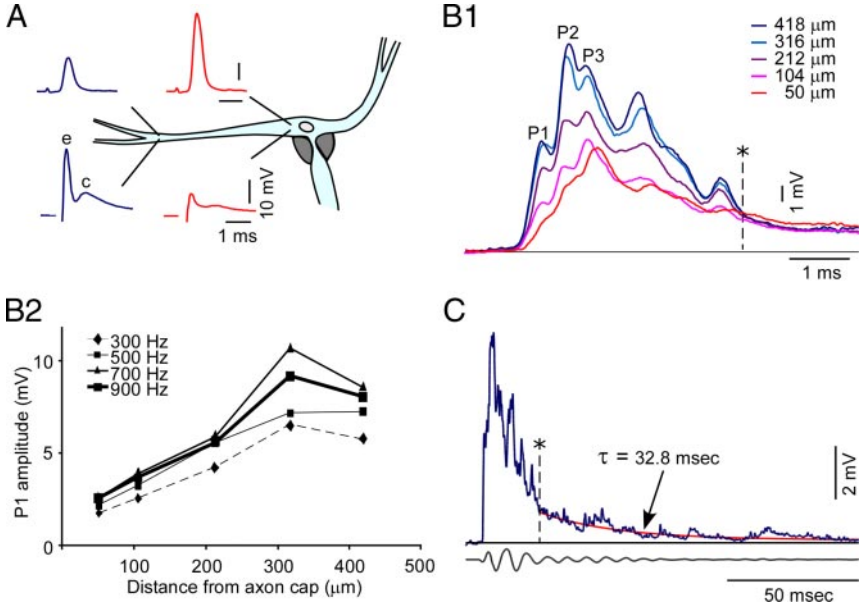

FIG. 3. Attenuation of sound-evoked EPSPs along the M-cell dendrite and soma. *A*: passive propagation of the antidromically evoked action potential and the EPSP evoked by VIIIth nerve stimulation, the latter of which has electrical (e) and chemical (c) synaptic components. Recordings were obtained 50 (*red*) and 350 μm (*blue*) lateral to the axon cap. *B1*: superimposed responses to a 700-Hz, 77-dB sound pip recorded at the indicated sites, showing attenuation of the EPSP from distal dendritic (*blue*) to proximal somatic (*red*) locations. P1, P2, P3, and the dashed vertical line (*) signify the first three peaks and the tail of the slow EPSP selected for quantitative measurements. *B2*: representative plots from one experiment of P1 amplitude at 5 recording sites along the lateral dendrite for the 4 indicated frequencies (same experiment illustrated in *B1*). *C*: sample recording illustrating slow PSP decay and superimposed exponential fit (*red*).

ning that region (Fig. 3, *B1* and *B2*). These results are consistent with a distal synaptic input in the region innervated by the large club endings and are not suggestive of a tonotopic map.

As mentioned in the preceding section, the fast EPSPs evoked by a pip are superimposed on a slow depolarizing envelope. One indicator of the "slow" EPSP is the slow decay of the EPSP after stimulus termination (Fig. 3, *B1* and *C*). The time constant of this decay (τ) was quantified using a single exponential fit of the EPSP tail. It averaged 33.43 ± 3.93 ms in the soma ($n = 26$) and 30.76 ± 3.76 ms in the dendrite [the amplitudes of the corresponding measurement starting points (e.g., * in Fig. 3, *B1* and *C*) were 1.87 ± 0.12 mV in the soma and 2.16 ± 0.23 mV in the dendrite; $n = 19$; NSD]. The possibility exists that residual sound reverberations contribute to the duration of the tail potential, but the absence of fast EPSPs in the composite M-cell response suggests this effect is minimal. Given that the M-cell membrane time constant is <0.5 ms, the slow decay of the EPSP is not ascribed to passive membrane properties, but instead either involves recruitment of a conductance change mechanism or reflects persistent afferent activity.

Pharmacological dissection of electrical and chemical components of EPSPs evoked by sound "pips"

The chemically mediated EPSP evoked in the M-cell by direct stimulation of VIIIp is glutamatergic, with both a small APV-sensitive component and a larger CNQX-sensitive component (Wolszon et al. 1997). We therefore asked whether antagonists to these receptors blocked any component of the sound-evoked EPSP recorded in the dendrite, using their effect on the EPSP evoked by direct nerve stimulation as a control (Fig. 4*A1*). This question is especially pertinent for the M-cell because the large majority of the club ending mixed synapses,

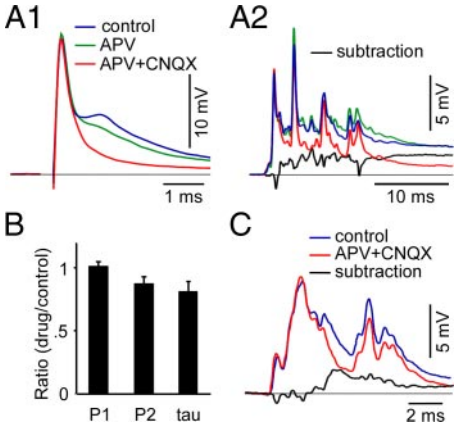

FIG. 4. Pharmacological evidence that the pip-evoked EPSP is predominantly mediated by electrical synapses. *A1* and *A2*: superimposed averaged dendritic responses evoked by VIIIp stimulation (*A1*) and a sound pip (*A2*: 200 Hz, 103 dB) recorded sequentially in saline (*blue*), saline with 100 μM APV (*green*), and saline with 100 μM CNQX (*red*). Difference between the responses in saline and in the presence of the 2 drugs is the underlying slow EPSP (subtraction, *black*). *B*: quantification of the effect of ionotropic glutamate receptor antagonist application. Reductions in P2 amplitude (13%; $P = 0.08$) and the tail potential decay (τ; 19%; $P = 0.18$) were not significant ($n = 6$). *C*: example from another experiment comparing the control (*blue*) and post-APV/CNQX (*red*) dendritic response to a sound pip (200 Hz, 84 dB). Subtraction of the latter from the control again demonstrates the presence of an underlying, slow EPSP (*black*).

when stimulated individually, are chemically silent (Lin and Faber 1988b). When strong posterior VIIIth nerve stimuli are used, the amplitude of the electrical EPSP recorded in the dendrite can be >25 mV, and then the size of the associated chemical EPSP is approximately one third that of the amplitude (Fig. 4*A1*). As shown in Fig. 4*A2*, individual fast EPSPs in the sound-evoked response, which are about 10 mV in amplitude in this case, do not appear to be followed by clear, chemically mediated EPSPs with kinetics and relative amplitudes comparable to the corresponding component in Fig. 4*A1*. Nevertheless, chemical EPSPs might have been less synchronized than with nerve stimulation and are thus masked by the complex sound response. However, when the brain was superfused with a cocktail of APV and CNQX (100 μM each), the values of P1, P2, and τ were at best slightly reduced compared with controls (Fig. 4*B*), and these effects were not significant (P1: $P = 0.35$; P2: $P = 0.08$; τ: $P = 0.18$; $n = 6$). This quantitative analysis demonstrated that the first peaks evoked in the dendrite by a sound pip are primarily mediated by distal electrotonic synapses and the decay of the slow EPSP is insensitive to ionotropic glutamate receptor antagonists.

Nevertheless, the AMPAR antagonists did reduce a component of the slow EPSP. For example, in the experiment of Fig. 4*A2*, superfusion with 100 μM APV had minimal effect, whereas subsequent application of 100 μM CNQX produced a clear decrease in the magnitude of the underlying slow EPSP. The APV/CNQX-sensitive component could be more clearly distinguished by subtracting the EPSP after drug application from the control EPSP (Fig. 4, *A2* and *C*). The difference signals began 1–3 ms after the EPSP onset and, in the example of Fig. 4*A2*, remained relatively constant for >20 ms. In the case of Fig. 4*C*, the drug-sensitive component also decayed more slowly ($\tau > 3$ ms) than the glutamatergic EPSP evoked by nerve stimulation ($\tau \approx 1.7$ ms). Thus there is a chemical component to the slow EPSP, but its characteristics differ from those of the example in Fig. 4*A1*.

M-cell responses evoked by amplitude- and frequency-modulated acoustic sounds

In natural habitats, fish are likely to be exposed not only to abrupt short sounds, such as a diving bird hitting the water, but also to longer-lasting stimuli. For example, an approaching predator will increase the intensity and frequency of its caudal fin beat during a strike (Wainwright et al. 2001). We thus asked whether a longer-duration ramped stimulus would reveal additional properties of the M-cell system. Specifically, two types of stimuli were generated: *1*) the constant frequency AM stimulus and *2*) the AM/FM stimulus. These stimuli were usually 50, 100, or 200 ms in duration.

In general, M-cell responses to AM and AM/FM stimuli consisted of a series of fast EPSPs superimposed on a steadily growing slow EPSP that gradually decayed back to baseline after termination of the sound (Fig. 5, *A–D*). These fast EPSPs were always largest in the dendrite, as indicated by RMS analysis of the high-pass (HP) filtered representation of the EPSP (HP RMS; dendrite: 0.73 ± 0.03 mV, $n = 16$, 32 responses; soma: 0.31 ± 0.01 mV, $n = 19$, 28 responses; $P < 0.005$, unpaired Student's *t*-test). These values correspond to a 58% attenuation in the fast EPSPs from distal dendrite to soma.

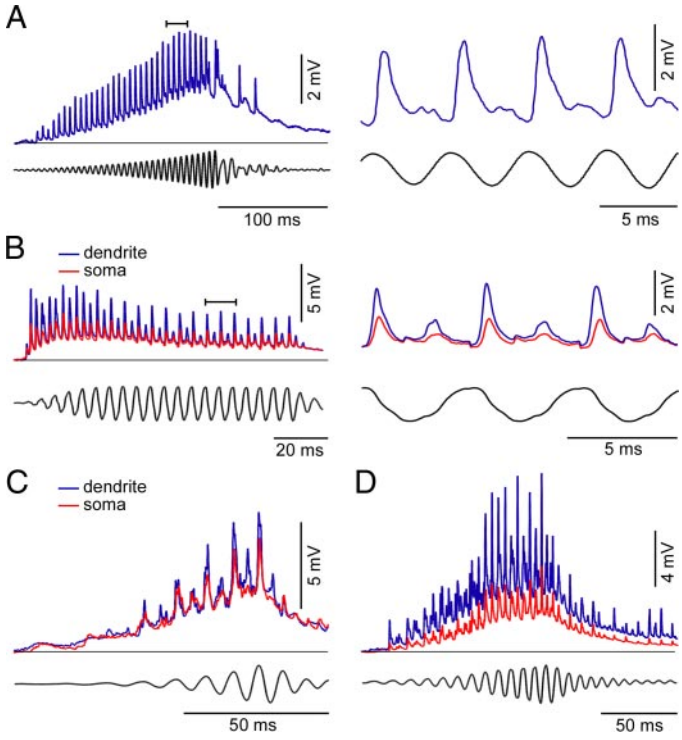

FIG. 5. Characterization of the M-cell response to modulated sound stimuli. *A*, *left*: an M-cell EPSP in response to an amplitude-modulated (AM) stimulus (200 Hz, 200 ms, 99 dB). Horizontal bar indicates the region in this response expanded (*right*) to demonstrate synchronization of the high-frequency EPSP component with the sound stimulus. *B*, *left*: superimposed somatic (*red*) and dendritic (*blue*) responses to a 200-Hz, 100-ms, 90-dB looming stimulus. Note: whereas the fast EPSPs were attenuated in the soma, the slow EPSP amplitude was constant from dendrite to soma. *B*, *right*: expansion of the indicated section of the response from the *left panel* (*black bar*) demonstrating synchronization of the fast EPSPs with sound frequency. *C* and *D*: superimposed somatic (*red*) and dendritic (*blue*) responses to a frequency-modulated (FM)/AM stimuli. *C*: EPSPs in response to a 50-Hz initial-frequency, 100-ms, 106.5-dB FM/AM stimulus. *D*: EPSPs in response to a 50-Hz initial frequency, 200-ms, 114-dB FM/AM stimulus. Note: both fast and slow EPSPs are attenuated in the soma.

In addition, the fast EPSPs appeared to follow the frequency of the sound and increase in amplitude with sound intensity (Fig. 5, *A* and *B*). Discrete chemical EPSPs following the fast EPSPs were not obvious (compare Fig. 4*A1* vs. Fig. 5, *A*, *right* and *B*, *right*).

The amplitude of the slow EPSPs evoked by these modulated sound stimuli also seemed to reflect changes in stimulus intensity, as shown in Fig. 5, *A–D*. In addition, whereas the amplitudes of the fast EPSPs were consistently attenuated from dendrite to soma, the slow EPSP was either isopotential throughout (Fig. 5, *B* and *C*) or was also clearly attenuated from dendrite to soma (Fig. 5*D*). To help quantify the spatial distribution of the slow EPSP, we low-pass filtered the composite M-cell response (Fig. 6, *A* and *B*). In three experiments where recordings were obtained from the dendrite and soma in the same cell (NSD), there was a 32 ± 2% attenuation of the slow component. In these experiments, the maximum amplitude of the low-pass signals (LP max) averaged 4.59 ± 0.68 mV (range: 0.8 to 8.4 mV) in the dendrite and 3.13 ± 0.37 mV (range: 1.2 to 5.1 mV) in the soma. Similarly, in data pooled from experiments where soma–dendrite recordings were made in different animals, LP max in the soma averaged 3.08 ± 0.13 mV (n = 19), which is 42% less than that in dendrite (LP max = 5.34 ± 0.28 mV; n = 16, $P < 0.005$, unpaired Student's t-test). In both sets of experiments, the attenuation of the slow EPSP is appreciably less than that of the fast EPSPs, which, as noted above, was 58% overall. Although this difference might seem to be consistent with the frequency dependency of the length constant of a passive cable (Jack et al. 1975), this is unlikely to be the cause of the difference in attenuation in these experiments because the M-cell membrane has a low specific resistance and time constant of about 0.5 ms (see model results below).

To quantify the kinetics of the slow EPSP in response to modulated sounds, its decay to baseline was examined. The low-pass–filtered signal was fit from peak to baseline with a double-exponential function ($A_1e^{-t/\tau_1} + A_2e^{-t/\tau_2}$), as illustrated in Fig. 6*A1* (*bottom traces*) for an EPSP evoked by a 200-ms AM stimulus. In these experiments, τ_1 averaged 25.1 ± 6.6 ms (n = 17, 32 responses) and 15.4 ± 2.7 ms (n = 15, 28 responses) in the soma and dendrite, respectively, and τ_2 was approximately four times slower, averaging 94.2 ± 7.5 ms in the soma and 106.6 ± 15.6 ms in the dendrite. Somatic and dendritic values of both τ_1 and τ_2 were not statistically different (τ_1: P = 0.18; τ_2: P = 0.47). Notably, the slow EPSPs evoked by the modulated stimuli decay appreciably more slowly than those evoked by pips (soma pip, τ = 33.43 ± 3.9 ms vs. soma modulated, τ_2 = 84.2 ± 10.1 ms; dendrite pip, τ = 30.76 ± 3.76 ms vs. dendrite modulated, τ_2 = 124.2 ± 23.1 ms).

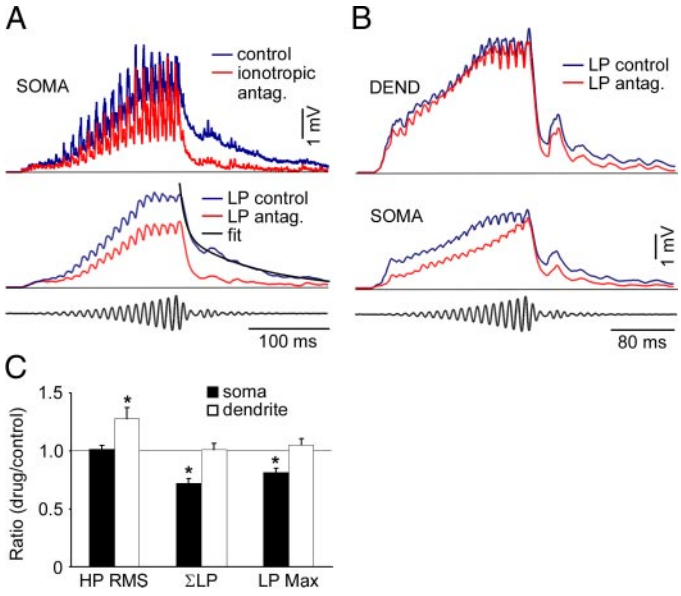

FIG. 6. Effects of glutamate receptor antagonists on EPSPs evoked by long-lasting modulated stimuli. *A*: M-cell responses in the soma (*top*) to an AM stimulus (*bottom*: 200 Hz, 100 ms, 90 dB) recorded before (*blue*) and after (*red*) superfusion with a cocktail of ionotropic glutamate receptor antagonists. *Middle traces*: corresponding low-pass–filtered representations before and after drug application. A double-exponential fit (*black*) is superimposed on the decay of the control low-pass signal (*blue*). *B*: low-pass–filtered responses to an AM stimulus (200 Hz, 100 ms, 90 dB) recorded from the dendrite (*top traces*) and soma (*middle traces*) of the same M-cell, respectively. *C*: histogram showing effects of ionotropic glutamate receptor antagonists on the 2 components of the sound-evoked EPSP: *1*) the root-mean-squared (RMS) value of the high-pass signal (HP RMS), representing the fast EPSP, and *2*) the maximum (LP max) and integrated area (Σ LP) of the low-pass signal, representing the slow EPSP.

Pharmacological dissection of electrical and chemical components of EPSPs evoked by AM and AM/FM sound stimuli

We next sought to determine whether the fast EPSPs arise solely from current flow across gap junctions at electrical synapses, as with the pips, and whether glutamatergic inputs contributed to the slow EPSP. To examine this, somatic and dendritic recordings of M-cell responses to long-lasting modulated sounds were again obtained before and after superfusion with an array of glutamate receptor antagonists. Antagonists of NMDA (200 μM APV, 100 μM CPP) and AMPA/kainate (150 μM CNQX, 100 μM NBQX) receptors were applied together to maximize their effectiveness. The ionotropic antagonists either had no effect on the size of the fast EPSPs (e.g., Fig. 6*A*) or actually increased them (Fig. 6*C*, HP RMS). More specifically, the drugs did not have a significant effect on the HP RMS voltage in the soma (1.2 $\pm$ 0.4% increase; $n = 12$, 19 responses; $P = 0.49$), although they did produce a nonspecific increase in the HP RMS in the dendrite (27.6 $\pm$ 9.8% increase; $n = 8$, 15 responses; $P < 0.05$). In contrast, the slow EPSP was reduced significantly in the case of somatic recordings, as confirmed with quantifications of the drug effects on the low-pass–filtered representations of the slow EPSP (Fig. 6*C*, $\sum$ LP and LP Max). Specifically, in the soma there was a significant blocking effect of the cocktail on both the integrated low-pass signal (28.0 $\pm$ 5.4% reduction; $P < 0.05$) and its peak amplitude (18.4 $\pm$ 3.4% reduction; $P < 0.05$), whereas the dendritic integrated low-pass signal (1.0 $\pm$ 5.2% reduction; $P = 0.87$) and peak amplitude (5.1 $\pm$ 5.5% increase; $P = 0.37$) were unaffected. This result is consistent with a predominantly proximal source of the glutamatergic component of the slow EPSP.

The data in Fig. 6 are from experiments in which either somatic or dendritic recordings were performed, but not both. To confirm these results, five additional experiments were performed in which recordings were obtained sequentially from the soma and the dendrite in the same preparation. In these experiments, the cocktail of AMPAR and NMDAR antagonists decreased LP max in the soma by 35 $\pm$ 4%, from 3.61 $\pm$ 0.49 mV ($P < 0.05$), compared with 17 $\pm$ 2% in the dendrite, from 5.17 $\pm$ 0.84 mV ($P = 0.05$). It should be noted that the peak amplitude of the experimentally recorded EPSP was unchanged after drug application (8.98 $\pm$ 0.92 vs. 8.52 $\pm$ 0.85 mV; $P = 0.46$; $n = 5$), resulting from a slight increase in the amplitude of the fast EPSPs that compensated for the reduced slow component. This increase in fast EPSP amplitude was most likely the result of a nonspecific increase in input resistance after drug application.

It is somewhat surprising that the glutamatergic antagonists did not have an effect on the slow EPSP recorded in the distal dendrite because the drug-sensitive component that is generated proximally should contribute to the response recorded distally, albeit with some attenuation arising from the passive cable properties of the dendrite. Ineffectiveness of the antagonists is unlikely, given that data are reported only for experiments in which the nerve-evoked chemical EPSP was blocked. A more likely explanation is that the dendritic representation of the proximally generated slow EPSP is a small fraction of the response recorded in the dendrite and the component removed by the antagonists is therefore relatively small. In confirmation, if experiments in which the integrated area of the low-pass–filtered PSP was reduced in the dendrite are considered separately (five of eight animals), the mean reduction in this measure was 10.8 $\pm$ 2.0% (nine responses).

Finally, control experiments demonstrated that a cocktail of AMPA and NMDA antagonists had negligible effects on synaptic transmission at hair cell–VIIIp afferent synapses. If this connection is blocked during drug application, it should result in decreased VIIIth nerve activity and, consequently, decreased fast EPSP amplitude. Therefore simultaneous recordings of extracellular activity in the afferent nerve and intracellular recordings of M-cell PSPs were performed ($n = 3$, 12 responses). In these experiments, cocktail application resulted in a 51 $\pm$ 5% reduction in the integrated area of the low-pass–filtered PSP ($\sum$ LP: $P < 0.0005$) and a 42 $\pm$ 6% reduction in LP max ($P < 0.0005$). In contrast, the RMS values of both the high-pass signal and the extracellular recordings were decreased by 19 $\pm$ 5% ($P < 0.005$) and 14 $\pm$ 5% ($P < 0.05$), respectively. Overall, these results indicate a greater effect on the magnitude of the slow EPSP than the fast EPSPs and thus a greater effect of the drugs on the VIIIp–M-cell synapse than the hair cell–VIIIp connection.

We also considered the possibility that a portion of the slow EPSP could be attributable to activation of metabotropic glutamate receptors (mGluRs). However, superfusion of the brain for $\leq$3 h with antagonists of Groups I, II, and III mGluRs (1 mM MSOP, 1 mM MCPG, and 200 μM LY 341495) did not reduce any EPSP component (data not shown; $n = 12$).

To summarize, although the slow EPSP is partially glutamatergic, evidence that the ionotropic antagonists had a proportionally greater effect on the responses recorded in the soma argues against a contribution of chemical synaptic inputs mediated by the large myelinated club endings that terminate on the distal lateral dendrite. Furthermore, discrete chemical EPSPs similar to those seen during direct VIIIp stimulation were not apparent in the sound-evoked responses and the decay kinetics of the slow EPSPs were at least one order of magnitude slower than those of the glutamatergic EPSPs evoked by VIIIp stimulation. Finally, the attenuation from dendrite to soma of this slow response was significantly less than that of the fast EPSPs.

Spatially distributed source of the slow EPSP

Because the difference in the spatial profile of the slow and fast EPSPs might have been a reflection of the frequency-dependent spatial-filtering properties of the dendrite, we implemented a multicompartment model to determine whether this was likely to be the case (see METHODS; Fig. 7, *top*).

We first modeled passive spread of the antidromic action potential along the dendrite. The somatically recorded action potential was injected into the model by a dynamic voltage clamp at 50 μm, and its predicted and observed amplitudes were compared at 100-μm intervals along the lateral dendrite (Fig. 7*A1*). Peak amplitudes of the experimental and modeled responses at 100, 200, 300, and 400 μm distal to the soma were not significantly different (for three data sets obtained from different M-cells; $P = 0.23$).

In a similar manner, EPSPs recorded in the distal dendrite were injected into the model, and the waveforms of predicted

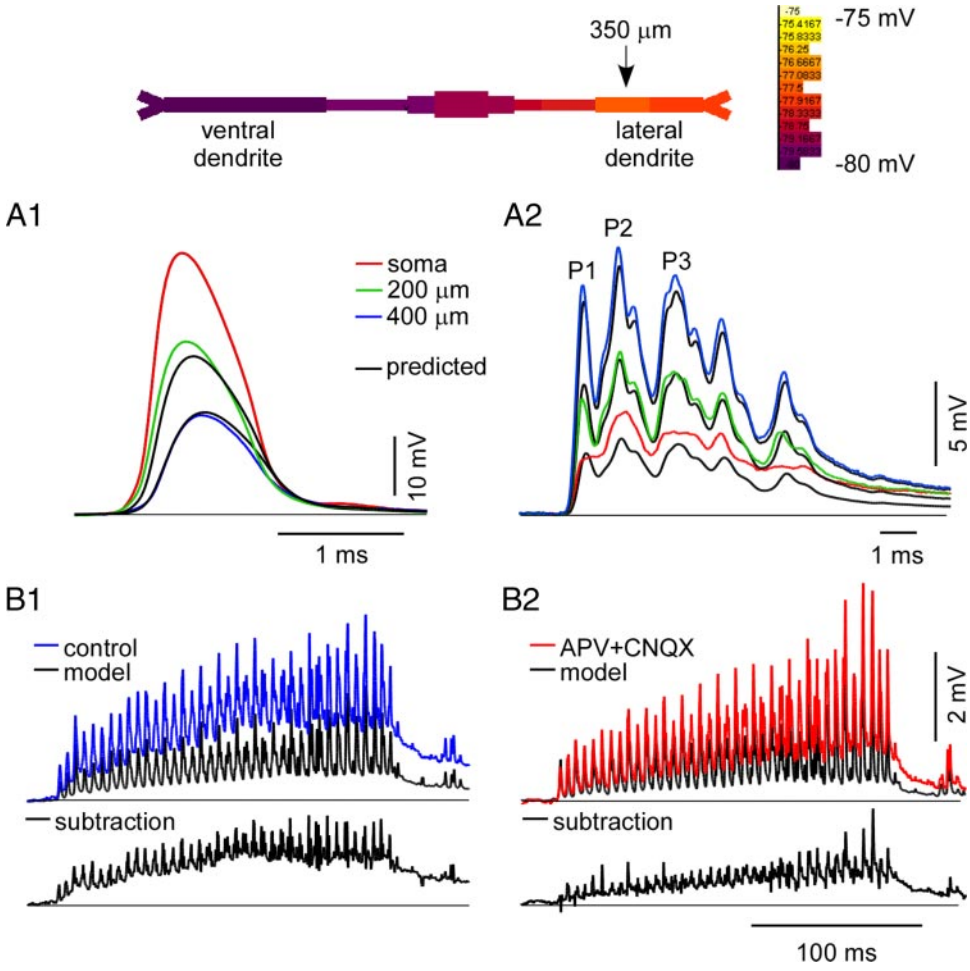

FIG. 7. Comparison of soma–dendritic attenuation of sound-evoked PSPs with predictions based on a passive multicompartment model of the M-cell. *Top*: representation of the model M-cell, color-coded to depict the spatial decay in amplitude of an EPSP from its dendritic source (350 μm, arrow) to the soma (for the response in *B1* at a time point 82 ms after response onset). *A1* and *A2*: validation of the model. *A1*: correspondence between antidromically evoked recordings of M-cell action potentials at 50 (soma, *red*), 200 (*green*), and 400 μm (*blue*) distal on the lateral dendrite, and the superimposed predicted dendritic waveforms (*black*), obtained by injecting the somatic response in dynamic voltage clamp at 50 μm (this record is not shown because, by definition, it is identical to the actual response). *A2*: similar comparison of experimental and predicted responses to a 300-Hz, 77-dB sound pip for the same experiment shown in *A1*. EPSP was injected by dynamic voltage clamp at 350 μm. Note the early equivalence of experimental and predicted EPSPs in the soma, and their divergence after P1. *B1* and *B2*: comparison of experimentally recorded somatic EPSPs evoked by a 100-Hz, 200-ms, 107-dB looming stimulus with modeled somatic EPSPs. [Note: the latter were predicted from experimental dendritic responses (not shown) where somatic and dendritic EPSPs were recorded in the same experiment before and after drug application.] Experimentally recorded dendritic EPSP was injected in the model dendrite at 350 μm. *B1*: superimposed experimental (*blue*) and modeled (*black*) control somatic responses. *B2*: superimposed experimental (*red*) and modeled (*black*) somatic responses after superfusion with an APV/CNQX cocktail. Note that the difference between the actual and predicted somatic waveforms (below, subtractions, *black*) was reduced in the presence of the cocktail.

and observed responses were compared at multiple locations. In the example of Fig. 7*A2*, the composite EPSP evoked by a 300-Hz sound pip recorded 400 μm distally on the lateral dendrite was injected into the model at 350 μm, the rationale being that sound-evoked EPSPs have approximately the same amplitude at 300 and 400 μm. At 200 μm, the model correctly predicted both the attenuation of the overall EPSP amplitude and the alterations in its shape. Although it also accurately predicted the amplitude of P1, i.e., the fast component, and the general shape of the response at 50 μm (soma), it significantly overestimated attenuation of the slow EPSP for all three data sets.

To further explore the origin and attenuation of the slow EPSP, the experimentally obtained average responses to a 100-Hz, 200-ms AM stimulus recorded in the distal dendrite before and after CNQX/APV application were injected into the model. The corresponding results are illustrated in Fig. 7, *B1* and *B2*, respectively. In both cases, the resulting modeled response in the soma underestimated the amplitude of the underlying slow EPSP recorded there ($n = 2$), but the discrepancy was approximately halved after CNQX/APV application. These results again suggest the existence of a proximal component to the slow EPSP that depends on activation of ionotropic glutamatergic transmission. Also, the component remaining after application of the antagonists does have a spatial profile consistent with a dendritic origin.

Spectral analysis of the sound-evoked EPSPs

The preceding data indicate that modulated acoustic stimuli evoke two types of EPSPs in the M-cell: fast, which are presumably mediated by electrical synapses, and slow, which apparently have a distributed origin. To determine the auditory information transmitted by these two distinct signals, we first asked to what extent the composite EPSPs followed stimulus frequency, and then separated them into their high- and low-frequency components.

The responses of one M-cell to 250- and 300-Hz AM stimuli are illustrated in Fig. 8, *A1* and *A2*, respectively. As already noted, the fast EPSPs grow in amplitude with the stimulus and are more closely spaced at the higher stimulus frequency. The power spectral densities of these EPSPs have, in addition to high power at low frequencies, sharp peaks at both the fundamental frequency and its first harmonic (Fig. 8*A3*). There was less power in the harmonic, consistent with the observation that in some experiments the amplitude of the fast EPSPs seemed to alternate; i.e., there were two peaks per stimulus cycle with the amplitude of the first at least twice that of the second (e.g., Fig. 5*B*). The latter is also consistent with previously reported results showing that auditory afferents fire once or twice per cycle depending on fiber type (Furukawa 1967). Overall, high-pass–filtered responses (>60 Hz) to AM stimuli ranging from 100 to 800 Hz were analyzed in 23 experiments, and in no case was power found outside of the range of the fundamental

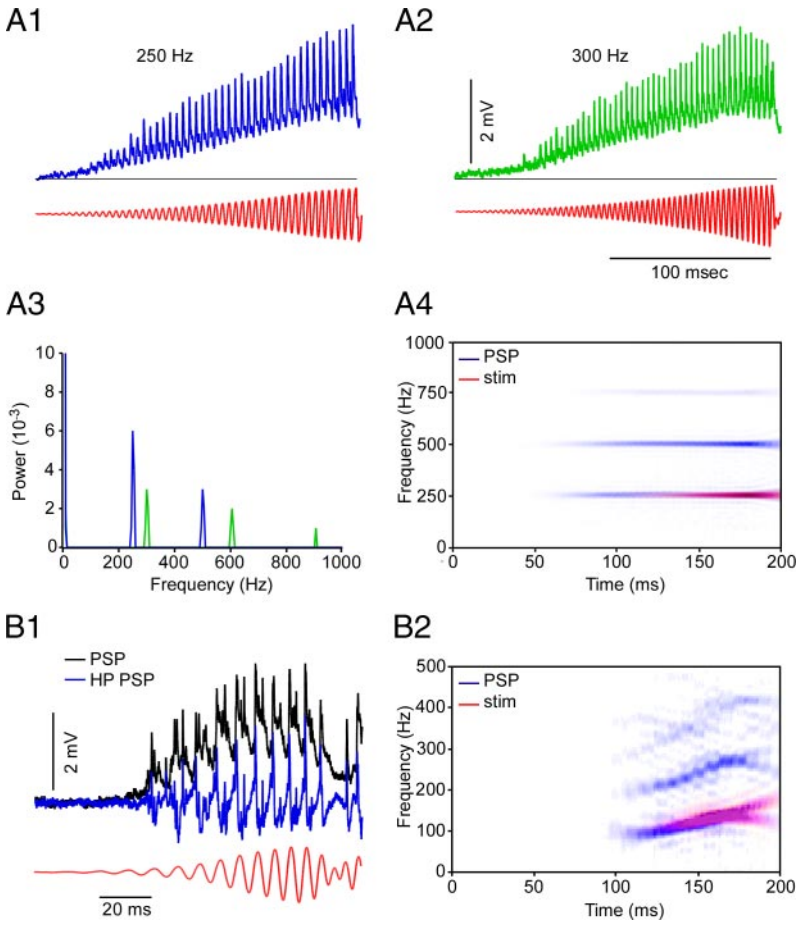

FIG. 8. Spectral analysis of M-cell responses to looming and FM/AM stimuli. *A1* and *A2*: EPSPs evoked in the M-cell soma by 250-Hz, 200-ms, 89-dB (*A1*, *blue*) and 300-Hz, 200-ms, 89-dB (*A2*, *green*) AM stimuli (*red*). *A3*: power spectral densities of the composite M-cell EPSPs illustrating high power in the low-frequency range (truncated peak) for the responses in *A1* and *A2* as well as sharp peaks at the fundamental frequencies and their first harmonics. *A4*: superimposed joint time–frequency spectrograms of the high-pass–filtered M-cell EPSP and the sound stimulus (same responses shown in *A1*). *B1*: somatic EPSP (*black*) evoked by a 200-ms FM/AM stimulus (50-Hz initial frequency, 109 dB, *red*). EPSP is superimposed on its high-pass–filtered representation (*blue*). *B2*: superimposed joint time–frequency spectrograms of the high-pass filtered M-cell response (*blue*) and the sound stimulus (*red*), demonstrating that the high-frequency component of the EPSP accurately follows the changing sound frequency and intensity.

frequency and its harmonics. The half-width of these spectral peaks was about 5 Hz (Fig. 8*A3*). Thus the high-frequency component of the EPSP accurately transmits information about the frequency of the sound. This was further illustrated by comparing the joint time-frequency spectrograms (JTFS) of the high-pass–filtered representation of the evoked responses and the corresponding sound stimuli, shown superimposed in Fig. 8*A4* for a 250-Hz AM stimulus. Another example of M-cell tracking can be seen in a sample response evoked by an AM/FM stimulus, which increases in both frequency and amplitude with time (Fig. 8, *B1* and *B2*). In both cases, superimposing the JTFS of the stimulus on that of the high-pass–filtered EPSP graphically demonstrates that the M-cell follows the fundamental frequency and its first harmonic of complex sounds, including for low intensities.

Separating EPSPs into their low- and high-pass–filtered components allowed us to ask quantitatively whether these components were sensitive to stimulus amplitude. This approach is illustrated in Fig. 9 for an EPSP recorded in the M-cell soma and evoked by a 250-Hz AM stimulus. The original EPSP and its low-pass–filtered signal are superimposed in Fig. 9*A1*, whereas Fig. 9, *A2* and *A3* illustrates the positive peak amplitude envelopes of the high-pass–filtered response and the sound stimulus, respectively. A comparison of the low-pass–filtered PSP with the amplitude envelope of the acoustic stimulus suggested they were correlated (Fig. 9*B*, *left*), as confirmed by linear regression analysis (Fig. 9*B*, *right*) of data from multiple experiments ($r^2 = 0.96 \pm 0.01$; $n = 12$; df = 93; $P < 0.0001$). A similar approach was implemented for the envelope of the high-pass EPSP representation (Fig. 9*C1*). The amplitude envelopes of the high-pass–filtered EPSP and the stimulus were not as well correlated ($r^2 = 0.70 \pm 0.02$; $n = 12$; df = 65; $P < 0.0001$). However, a stronger correlation was demonstrated between the high-pass–filtered EPSP power and stimulus intensity, i.e., the square of the amplitude ($r^2 = 0.95 \pm 0.02$; $n = 12$; df = 174; $P < 0.0001$; Fig. 9*C2*), indicating that the fast component of the PSP also tracks stimulus amplitude. The slopes of the linear regressions were frequency dependent, with the greatest sensitivity in the range of 250 to 400 Hz. These results indicate that the slow EPSP provides a tonic representation of the amplitude of the stimulus, whereas the fast EPSPs provide a phasic representation of the stimulus amplitude at a rate dependent on the frequency of the stimulus.

DISCUSSION

The major findings of the present study of acoustic information transmitted by synapses between auditory afferents and the M-cell are that *1*) this information is separated into two components, one that is phasic and phase-locked to stimulus frequency and its first harmonic and one that is slower and rather tracks the amplitude envelope of the stimulus; *2*) the fast component of the postsynaptic response evoked by both the brief pips and the prolonged ramped sounds is a series of fast electrotonic coupling potentials arising from synchronous presynaptic activity in the large myelinated club endings that terminate on the distal lateral dendrite of the M-cell; *3*) the

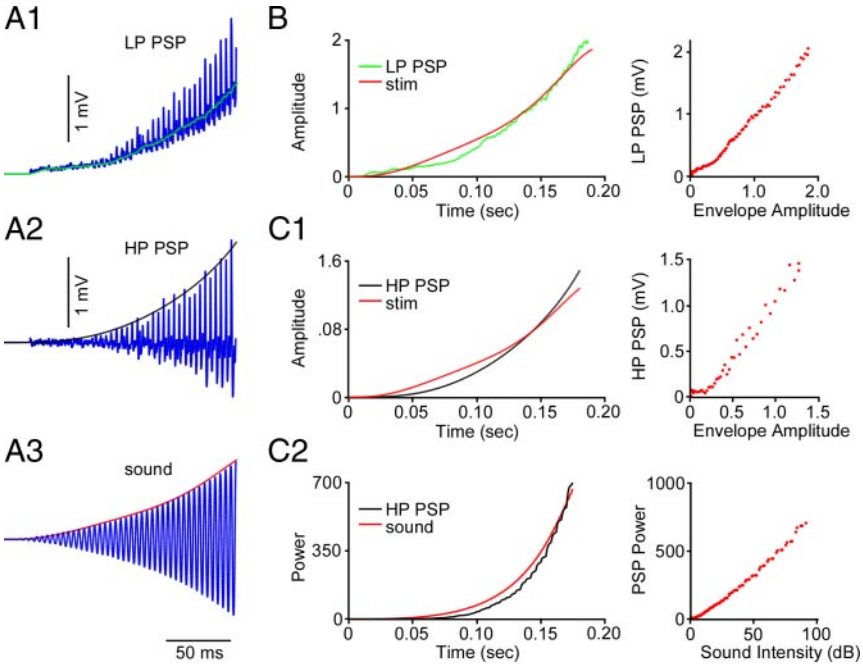

FIG. 9. Correlations between the EPSP components and dynamic stimulus parameters: representative analysis from one experiment. *A1–A3*: separation of the composite EPSP evoked in the M-cell soma by a 200-Hz, 100-ms, 89-dB looming stimulus (*A3*) into its low-pass (*A1*) and high-pass (*A2*) components. *A1*: composite EPSP (*blue*) and the superimposed low-pass–filtered fit (*green*). *A2*: high-pass–filtered EPSP (*blue*), with the fit of its peak amplitudes superimposed (*black*). *A3*: sound stimulus (*blue*) and the polynomial fit of its envelope (*red*). *B*: plots of the fits of the low-pass–filtered EPSP and the scaled sound amplitude envelope vs. time (*left*) and the corresponding linear regression (*right*: $r^2 = 0.992$; $P < 0.0001$). *C1*: plots of the fits of the high-pass–filtered EPSP amplitude and the scaled sound amplitude envelope vs. time (*left*) and the corresponding linear regression (*right*: $r^2 = 0.701$; $P < 0.0001$). *C2*: plots of the power of the high-pass–filtered EPSP vs. the intensity (amplitude squared) of the sound signal (*left*) and the corresponding linear regression (*right*: $r^2 = 0.994$; $P < 0.0001$).

underlying slow EPSP is more prominent when longer-lasting amplitude- and frequency-modulated sounds are applied; and *4*) this slow EPSP has both proximal and distal sources, with only the proximal component being sensitive to glutamatergic antagonists. These two classes of responses, fast and slow EPSPs, appear to have overlapping, complementary functions because they both encode a measure of stimulus intensity, while only the fast EPSP encodes frequency. In addition, the properties of the slow EPSP evoked by the modulated stimuli as well as its amplitude distribution along the soma–dendritic membrane are not characteristic of glutamatergic EPSPs mediated by the club ending synapses on the distal dendrite (Lin and Faber 1988a). These results suggest the chemical component of these morphologically mixed synapses was weak or even functionally silent in the present experimental conditions (Lin and Faber 1988a,b).

Phasic EPSPs are mediated by electrotonic synapses

Evidence is accumulating that electrical synapses might be more widespread in the vertebrate CNS than previously recognized (Nagy et al. 2004). Our conclusion that fast EPSPs are electrical coupling potentials is based on *1*) their kinetics, *2*) their insensitivity to AMPAR and NMDAR antagonists, and *3*) their spatial profiles along the soma–dendritic cable that are consistent with a distal dendritic origin. These coupling potentials have the same half-width (i.e., time course) as that of the presynaptic spikes in this system because the M-cell membrane time constant is so short. Consequently, the electrical synapses faithfully follow stimulus frequency, up to about 1,000 Hz (data not shown). The notion that the electrotonic synapses act as high-pass filters of auditory signals might be unique to the M-cell system, although such a role was previously observed in the electrosensory system of mormyid electric fish (Bell and Grant 1989; reviewed in Carr and Friedmann 1999). In other systems, such as mammalian cortex and hippocampus, electrotonic coupling between interneurons is very weak and longer membrane time constants slow potentials and distort their waveforms (see Connors and Long 2004). The coupling in these systems seems to aid in synchronizing firing patterns and its role in information processing is less clear. This functional difference would appear to parallel the differences in the type of coupling: cortical and hippocampal coupling is between homologous cell types, and there are no clear pre- and postsynaptic elements, in contrast to the electrical synapses between afferents and identified target neurons in the M-cell case and in the electrosensory lateral line system of Gymnotids.

Distributed origin of the slow EPSP

Previous studies using paired pre- and postsynaptic recordings indicated that at least 80% of M-cell afferent synapses are chemically silent when activated in isolation (Lin and Faber 1988b), but might be unblocked when a population of fibers is coactivated synchronously (Pereda et al. 2004). For example, a clear chemical EPSP is recorded in the dendrite when the preceding coupling potential has an amplitude in the range of 20 mV. Results using sound pips revealed a small glutamatergic component with a longer latency and kinetics slower than those of unitary EPSPs (e.g., Fig. 4*C*). We used longer-lasting, modulated acoustic stimuli, that is, those that triggered escapes in behavioral studies when applied under water (unpublished observations) and asked whether chemical synaptic transmission might be more prominent in those conditions. These paradigms revealed larger, slow postsynaptic responses that had no significant NMDAR component, despite the fact that the slow EPSP amplitude was in the range where EPSPs evoked by VIIIp stimulation are sensitive to NMDAR blockers (Wolszon et al. 1997). In addition, the slow EPSPs were only partially blocked by the ionotropic glutamate receptor antagonists, and their rates of rise and decay were one to two orders of magnitude slower than those of chemically mediated EPSPs evoked by direct nerve stimulation. Although the spatial distribution of the fast EPSP was consistent with a purely distal

dendritic source, this was not the case for the slow EPSP. In some experiments, the slow EPSP amplitude was maximal in the distal dendrite, whereas in others it was the same size in the soma as in the dendrite. The latter case is consistent with a combination of distal and proximal sources. Even when the slow EPSP was maximal distally, its decrement from dendrite to soma was less than that predicted by a multicompartment model of the cell that both reproduced the measured input resistance and time constant of the M-cell, as well as satisfactorily fit the temporal and spatial profile of the fast electrical EPSPs and the antidromic spike. This discrepancy between predicted and observed cable properties was seen only with the attenuation of the slow EPSP from dendrite to soma, especially before superfusion with a cocktail of the ionotropic glutamatergic blockers. Furthermore, the cocktail of antagonists was most effective on responses recorded in the soma and least effective at the dendrite. These observations are consistent with the notion of a proximal glutamatergic source to the slow EPSP and a more distal nonglutamatergic component.

It is important to note that because acoustic stimuli were applied in air, the evoked PSPs were presumably smaller than those that trigger an M-cell spike and an escape behavior when comparable underwater stimuli are used. It is not clear whether the underwater stimulus has a larger pressure component and therefore synchronously activates more posterior VIIIth nerve afferents. Thus that is one possible condition in which the club endings would mediate not only electrical but also chemical PSPs. Furthermore, if the mechanism that unblocks chemical transmission is a result of feedback of M-cell dendritic depolarizations to the presynaptic terminals via the gap junctions (Pereda et al. 2004), an additional source of that depolarization could be PSPs mediated by other eighth nerve or lateral line afferents that are sensitive to different components of an acoustic stimulus.

The most likely source of the proximal input is a mono- or disynaptic input from saccular or lagenar afferents, different from the fibers that give rise to the large myelinated club endings. Previous morphological studies have not provided evidence for such a monosynaptic input (Zottoli 1978), suggesting that a disynaptic pathway is more likely. Indeed, the interposition of interneurons might account for the lack of evidence for discrete time-locked chemical EPSPs.

Potential mechanisms underlying the distal component of the slow EPSP

The source of the residual slow EPSP that persists following application of the ionotropic glutamatergic antagonists is less clear. We considered the possibility that synaptic activation of a metabotropic glutamate receptor (Coutinho and Knopfel 2002; Knopfel and Grandes 2002) might be involved, but the failure to detect any blocking effect with a broad spectrum of mGluR antagonists suggests that is not the case. The most likely alternative is electrotonic transmission of slow potentials generated in the VIIIp afferents. The afferent spikes have depolarizing afterpotentials, as reflected in the isolated coupling potential waveform in Fig. 4*A1*, and successive depolarizations may summate. The afferents also exhibit a voltage-dependent persistent Na^+ current (Curti and Pereda 2004) that might produce a slowly developing depolarization of the afferents, which would in turn spread to the lateral dendrite. However, this nonlinearity might be offset during maintained or repetitive presynaptic depolarization by an opposing action of voltage-dependent K^+ channels. Another source of a presynaptic slow potential would be the chemical synapses between sensory hair cells and the afferents. The length constant of the afferents seems to be sufficiently long for such a signal to spread to the M-cell because efferent IPSPs generated at the hair cell synapses can be recorded in the afferents close to the site of entry in the brain (Lin and Faber 1988c). Finally, we consider a subthreshold, voltage-dependent nonlinearity of the dendritic membrane to be less likely. The only nonlinearity described thus far is an instantaneous inward rectification that is manifest as a decreased input conductance at depolarizations 5 to 10 mV above the M-cell resting potential (Faber and Korn 1986). This conductance deactivates more rapidly than the slow EPSP, however, and neither voltage-clamp nor current-clamp experiments have unmasked evidence for a subthreshold inward current with the appropriate kinetics. Regardless, we suggest that, in addition to the proximal glutamatergic input to the M-cell, a major component of the slow EPSP is transmitted to the M-cell via electrical synapses, as is also the case for the fast EPSP.

Functional significance and behavioral relevance of the EPSP components

Both the abrupt "pip" and the more gradual modulated stimuli used in this study can evoke escapes when applied under water. Although the stimuli in air produce the same pressure waves as those in water, they do not generate the other component of sound in water, that is, particle displacement or acceleration (Popper and Fay 1999). This difference most likely explains why the PSPs we recorded were not large enough to trigger an M-cell action potential. We also considered the alternative explanation: that the anesthetic MS-222 reduced the PSP magnitude or altered its waveform. However, data from Palmer and Mensinger (2004) suggests the anesthetic has minimal effect on this afferent pathway at the concentration used. In confirmation, we conducted an institutionally approved pilot study in which two fish were initially anesthetized by immersion in ice water and local anesthetic (20% benzocaine gel, Ultradent) was applied topically to the skull and all contact points before restraining the fish. The EPSP waveforms and magnitude were comparable to those in the experiments described here, and addition of MS-222 (60 μg/l) to the water perfusing the gills had minimal effect on the evoked responses. We thus conclude that the PSPs described here are representative of those that can trigger an escape and that in order to reach threshold for that behavior, these responses summate with those mediated by the other afferent pathways; i.e., by VIIIth nerve afferents excited by the displacement component of underwater acoustic stimuli and, possibly, by lateral line afferents (Mirjany et al. 2005).

In the auditory system of a range of vertebrates, and in fish electrosensory systems, sensory information is separated into two coding channels specialized for phase detection and stimulus amplitude tracking (Carr and Friedman 1999). In the mammalian auditory system, the kinetics of glutamatergic EPSCs allows them to follow high-frequency inputs and therefore have a role in phase detection (Otis et al. 1995; Raman et al. 1994). In contrast, our results suggest that the two coding

channels converge at the M-cell level, and that the fast EPSP is mediated by electrical synapses on the M-cell and encodes stimulus frequency and intensity, whereas the slow EPSP converts a phasic input into a tonic signal that is proportional to the envelope of peak stimulus amplitude. These two aspects of a threatening stimulus, intensity and frequency, are both functionally relevant. Intensity and its rate of change are measures of the size of an approaching object and its speed. In the case of frequency and associated phase-related information, it has been postulated that these parameters are important in determining the directionality of the escape behavior, particularly in the case of stimuli directly to one side or the other [i.e., in selecting which M-cell will fire an action potential (Casagrand et al. 1999)]. Thus the M-cell and its afferent network are well suited for retaining information about the dynamic properties of complex stimuli. Indeed, it has been suggested previously that information coding in the CNS is optimized for an efficient representation of dynamic and complex signals from the environment (Barlow 1961; Machens et al. 2005), a principle that apparently is realized for sound-evoked responses in the M-cell. Moreover, we suggest the separation of an incoming signal into two different information channels might be a common function of neural networks that use electrical synapses. Differential coding properties have been suggested for electrical and chemical synapses between proprioceptive afferents and interneuron A in the crayfish (Nagayama et al. 1997), although the functions have not been delineated.

Although stimulation of the eighth nerve also activates a feedforward inhibition of the M-cell (Faber et al. 1989), we have not considered its role here and have focused on the composite EPSPs. Theoretically, however, inhibition could shunt the magnitude of the fast EPSPs and produce frank hyperpolarizations as the slow EPSP reaches its peak. In fact, it might contribute to the initial fast decay (τ_1) of the slow EPSP or to the alternation in the amplitudes of successive fast EPSPs. In addition, it will be important to determine whether inhibition shapes the input–output relations of the fast and slow PSPs, as well as how it influences the correlations between these responses and stimulus intensity or power.

The escape response initiated by an M-cell action potential can be triggered by sound pips as well as by longer-lasting amplitude- and frequency-modulated sounds. These stimuli represent environmental perturbations potentially produced by a variety of predatory activities (Bleckmann et al. 1991). For example, an approaching predator might alter its fin movements and swimming velocity—sometimes even producing suction—during a strike (Wainwright et al. 2001; Webb 1976). These behaviors activate multisensory inputs to the M-cell (Popper and Fay 1999), and although the pressure input, transmitted by the swim bladder to the posterior eighth nerve, is necessary for the escape behavior (Canfield and Eaton 1990), it presumably is insufficient to trigger the escape by itself (Casagrand et al. 1999). In fact, the input from the swim bladder imparts to certain fish, such as goldfish, the designation of hearing specialists; that is, it underlies their particular sensitivity to sound (Fay and Popper 1999). The composite EPSPs evoked by the modulated stimuli used in this study appear to aid the integrative requirements for the escape behavior. Although the phasic component tracks stimulus intensity and frequency, the tonic signal increases the chances that the M-cell reaches threshold when inputs from multiple sources are summed; i.e., the fast EPSP alone accurately follows sound frequency or its first harmonic and therefore favors a threshold mechanism based on temporally coincident, or convergent, input signals. However, the slow EPSP is a more slowly modulated signal that therefore presumably reduces or relaxes this requirement for coincident inputs. That is, the slow EPSP might allow for summation of inputs on a broader timescale than the faster responses, whose waveforms are comparable to those of the presynaptic action potentials. This could be very important in situations where the escape response is triggered by multimodal sensory inputs; for example, a combination of acoustic and visual stimuli.

GRANTS

This work was supported by National Institute of Neurological Disorders and Stroke Grant NS-15335 to D. S. Faber.

REFERENCES

Barlow HB. Possible principles underlying the transformation of sensory messages. In: *Sensory Communications*, edited by Rosenblith WA. Cambridge, MA: MIT Press, 1961, p. 217–234.

Bell CC and Grant K. Corollary discharge inhibition and preservation of temporal information in a sensory nucleus of mormyrid electric fish. *J Neurosci* 9: 1029–1044, 1989.

Bennett MV and Zukin RS. Electrical coupling and neuronal synchronization in the mammalian brain. *Neuron* 41: 495–511, 2004.

Bleckmann H, Breithaupt T, Blickhan R, and Tautz J. The time course and frequency content of hydrodynamic events caused by moving fish, frogs and crustaceans. *J Comp Physiol A Sens Neural Behav Physiol* 168: 749–757, 1991.

Bodian D. Introductory survey of neurons. *Cold Spring Harb Symp Quant Biol* 17: 1–13, 1952.

Canfield JG and Eaton RC. Swimbladder acoustic pressure transduction initiates Mauthner-mediated escape. *Nature* 347: 760–762, 1990.

Carr CE and Friedman MA. Evolution of time coding systems. *Neural Comput* 11: 1–20, 1999.

Casagrand JL, Guzik AL, and Eaton RC. Mauthner and reticulospinal responses to the onset of acoustic pressure and acceleration stimuli. *J Neurophysiol* 82: 1422–1437, 1999.

Connors BW and Long MA. Electrical synapses in the mammalian brain. *Annu Rev Neurosci* 27: 393–418, 2004.

Coutinho V and Knopfel T. Metabotropic glutamate receptors: electrical and chemical signaling properties. *Neuroscientist* 8: 551–561, 2002.

Curti S and Pereda AE. Voltage-dependent enhancement of electrical coupling by a subthreshold sodium current. *J Neurosci* 24: 3999–4010, 2004.

Edwards DH, Yeh SR, and Krasne FB. Neuronal coincidence detection by voltage-sensitive electrical synapses. *Proc Natl Acad Sci USA* 95: 7145–7150, 1998.

Faber DS, Fetcho JR, and Korn H. Neuronal networks underlying the escape response in goldfish. *Ann NY Acad Sci* 563: 11–33, 1989.

Faber DS and Korn H. Electrophysiology of the Mauthner cell: basic properties, synaptic mechanisms and associated networks. In: *Neurobiology of the Mauthner Cell*, edited by Faber DS and Korn H. New York: Raven Press, 1978, p. 47–131.

Faber DS and Korn H. Instantaneous inward rectification in the Mauthner cell: a postsynaptic booster for excitatory inputs. *Neuroscience* 19: 1037–1043, 1986.

Fay RR and Popper AN. Hearing in fishes and amphibians: an introduction. In: *Comparative Hearing: Fish and Amphibians*, edited by Fay RR and Popper AN. New York: Springer-Verlag, 1999, p. 43–100.

Furukawa T. Synaptic interaction at the Mauthner cell of goldfish. *Prog Brain Res* 21: 44–70, 1966.

Furukawa T and Furshpan EJ. Two inhibitory mechanisms in the Mauthner neurons of goldfish. *J Neurophysiol* 26: 140–176, 1963.

Furukawa T and Ishii Y. Neurophysiological studies on hearing in goldfish. *J Neurophysiol* 30: 1377–1403, 1967.

Jack JJB, Noble D, and Tsien RW. *Electric Current Flow in Excitable Cells*. New York: Oxford Univ. Press, 1975.

Johnson BR, Peck JH, and Harris-Warrick RM. Dopamine induces sign reversal at mixed chemical-electrical synapses. *Brain Res* 625: 159–164, 1993.

Kepler TB, Marder E, and Abbott LF. The effect of electrical coupling on the frequency of model neuronal oscillators. *Science* 248: 83–85, 1990.

Knopfel T and Grandes P. Metabotropic glutamate receptors in the cerebellum with a focus on their function in Purkinje cells. *Cerebellum* 1: 19–26, 2002.

Lin JW and Faber DS. Synaptic transmission mediated by single club endings on the goldfish Mauthner cell. I. Characteristics of electrotonic and chemical postsynaptic potentials. *J Neurosci* 8: 1302–1312, 1988a.

Lin JW and Faber DS. Synaptic transmission mediated by single club endings on the goldfish Mauthner cell. II. Plasticity of excitatory postsynaptic potentials. *J Neurosci* 8: 1313–1325, 1988b.

Lin JW and Faber DS. An efferent inhibition of auditory afferents mediated by the goldfish Mauthner cell. *Neuroscience* 24: 829–836, 1988c.

Lin JW, Faber DS, and Wood MR. Organized projection of the goldfish saccular nerve onto the Mauthner cell lateral dendrite. *Brain Res* 274: 319–324, 1983.

Machens CK, Gollisch T, Kolesnikova O, and Herz AV. Testing the efficiency of sensory coding with optimal stimulus ensembles. *Neuron* 47: 447–456, 2005.

Mirjany M, Faber DS, and Preuss T. The role of the lateral line in the goldfish escape response. Program No. 77.1. *2005 Abstract Viewer and Itinerary Planner.* Washington, DC: Society for Neuroscience, CD-ROM, 2005.

Nagayama T, Aonuma H, and Newland PL. Convergent chemical and electrical synaptic inputs from proprioceptive afferents onto an identified intersegmental interneuron in the crayfish. *J Neurophysiol* 77: 2826–2830, 1997.

Nagy JI, Dudek FE, and Rash JE. Update on connexins and gap junctions in neurons and glia in the mammalian nervous system. *Brain Res Brain Res Rev* 47: 191–215, 2004.

Oda Y, Kawasaki K, Morita M, Korn H, and Matsui H. Inhibitory long-term potentiation underlies auditory conditioning of goldfish escape behavior. *Nature* 394: 182–185, 1998.

Otis TS, Raman IM, and Trussell LO. AMPA receptors with high Ca^{2+} permeability mediate synaptic transmission in the avian auditory pathway. *J Physiol* 482: 309–315, 1995.

Palmer LM and Mensinger AF. Effect of the anesthetic tricaine (MS-222) on nerve activity in the anterior lateral line of the oyster toadfish, *Opsanus tau*. *J Neurophysiol* 92: 1034–1041, 2004.

Pereda AE, Rash JE, Nagy JI, and Bennett MVL. Dynamics of electrical transmission at club endings on the Mauthner cells. *Brain Res Brain Res Rev* 47: 227–244, 2004.

Popper AN and Fay RR. The auditory periphery in fishes. In: *Comparative Hearing: Fish and Amphibians*, edited by Fay RR and Popper AN. New York: Springer-Verlag, 1999, p. 43–100.

Popper AN and Platt C. Inner ear and lateral line. In: *The Physiology of Fishes*, edited by Evans DH. Boca Raton, FL: CRC Press, 1993, p. 99–136.

Preuss T and Faber DS. Central cellular mechanisms underlying temperature-dependent changes in the goldfish startle-escape behavior. *J Neurosci* 23: 5617–5626, 2003.

Raman IM, Zhang S, and Trussell LO. Pathway-specific variants of AMPA receptors and their contribution to neuronal signaling. *J Neurosci* 14: 4998–5010, 1994.

Segev I and Burke RE. Compartmental models of complex neurons. In: *Methods in Neuronal Modeling: From Ions to Networks* (2nd ed.), edited by Segev I and Koch C. Cambridge, MA: MIT Press, 1998, p. 112–113.

Sharp AA, Abbott LF, and Marder E. Artificial electrical synapses in oscillatory networks. *J Neurophysiol* 67: 1691–1694, 1992.

Thomson AM. Neurotransmission: chemical and electrical interneuron coupling. *Curr Biol* 10: R110–R112, 2000.

Tuttle R, Masuko S, and Nakajima Y. Freeze-fracture study of the large myelinated club ending synapse on the goldfish Mauthner cell: special reference to the quantitative analysis of gap junctions. *J Comp Neurol* 246: 202–211, 1986.

Wainwright PC, Ferry-Graham LA, Waltzek TB, Carroll AM, Hulsey CD, and Grubich JR. Evaluating the use of ram and suction during prey capture by cichlid fishes. *J Exp Biol* 204: 3039–3051, 2001.

Webb PW. The effect of size on the fast-start performance of rainbow trout *Salmo cairdneri*, and a consideration of piscivorous predator–prey interactions. *J Exp Biol* 65: 157–177, 1976.

Wolszon LR, Pereda AE, and Faber DS. A fast synaptic potential mediated by NMDA and non-NMDA receptors. *J Neurophysiol* 78: 2693–2706, 1997.

Zottoli SJ. Correlation of the startle reflex and Mauthner cell auditory responses in unrestrained goldfish. *J Exp Biol* 66: 243–254, 1977.

Zottoli SJ. Comparative morphology of the Mauthner cell in fish and amphibians. In: *Neurobiology of the Mauthner Cell*, edited by Faber DS and Korn H. New York: Raven Press, 1978, p. 13–45.

Zottoli SJ and Faber DS. The Mauthner cell: what has it taught us? *Neuroscientist* 6: 25–37, 2000.